

Kinematics and Structure of Clumps in Broad-line Regions in Active Galactic Nuclei

Mohammad Ghayuri*

Independent Scholar, Mashhad, Iran

ABSTRACT

We use the Jeans equations for an ensemble of collisionless particles to describe the distribution of broad-line region (BLR) cloud in three classes: (A) non disc (B) disc-wind (C) pure disc structure. We propose that clumpy structures in the brightest quasars belong to class A, fainter quasars and brighter Seyferts belong to class B, and dimmer Seyfert galaxies and all low-luminosity AGNs (LLAGNs) belong to class C. We derive the virial factor, f , for disc-like structures and find a negative correlation between the inclination angle, θ_0 , and f . We find similar behaviour for f as a function of the FWHM and σ_z , the z component of velocity dispersion. For different values of θ_0 we find that $1.0 \lesssim f \lesssim 9.0$ in type1 AGNs and $0.5 \lesssim f \lesssim 1.0$ in type2 AGNs. Moreover we have $0.5 \lesssim f \lesssim 6.5$ for different values of FWHM and $1.4 \lesssim f \lesssim 1.8$ for different values of σ_z . We also find that f is relatively insensitive to the variations of bolometric luminosity and column density of each cloud and the range of variation of f is in order of 0.01. Considering wide range of f we see the use of average virial factor $\langle f \rangle$ is not very safe. Therefore We propose AGN community to divide a sample into a few subsamples based on the value of θ_0 and FWHM of members and calculate $\langle f \rangle$ for each group separately to reduce uncertainty in black hole mass estimation.

Key words: galaxies: active - galaxies: nuclei - galaxies: Seyfert - galaxies: kinematics and dynamics - black hole physics

1 INTRODUCTION

Now it is widely accepted that an active galactic nucleus (AGN) is a supermassive black hole surrounded by an accretion disc. Above the accretion disc, there is dense, rapidly-moving gas making up the so-called broad line region (BLR) emitting broad emission lines by reprocessing the continuum radiation from the inner accretion disc (see Gaskell 2009). The BLR is believed to consist of dense clumps of hot gas ($n_H > 10^9 \text{ cm}^{-3}$; $T \sim 10^4 \text{ K}$) in a much hotter, rarefied medium. The motions of the line-emitting clouds is the main cause of the broadening of the line profiles.

The profiles of the broad emission lines is a major source of information about the geometry and kinematics of the BLR. Profiles can be broadly categorized into two shape: single-peaked and double-peaked. It is believed that double-peaked profiles are emitted from disc-like clumpy structure (e.g., Chen et al. 1989; Chen & Halpern 1989; Eracleous & Halpern 1994, 2003; Strateva et al. 2003). Although obvious double-peaked profiles are seen in only small fraction of AGNs, this does not mean that such discs are absent in other AGNs. Based on some studies, under the specific conditions, disc-like clumpy structure can even produce

single-peaked broad emission lines (e.g., Chen & Halpern 1989; Dumont & Collin-Souffrin 1990a; Kollatschny & Bischoff 2002; Kollatschny 2003). Spectropolarimetric observations (Smith et al. 2005) imply the presence of clumpy discs in BLR. On the other hand, other authors have suggested a two-component model in which they consider a spherical distribution of clouds surrounding the central black hole in addition to their distribution in the midplane (e.g., Popovic et al. 2004; Bon et al. 2009). In this model, while the disc is responsible for the production of the broad wings, the spherical distribution is responsible for the narrow cores. The integrated emission line profile is a combination of wings and cores.

Using the width of the broad Balmer emission lines, FWHM, and an effective BLR radius, r_{BLR} , which is obtained by either reverberation mapping (RM) (e.g., Blandford & McKee 1982; Gaskell & Sparke 1986; Peterson 1993; Peterson et al. 2004) or from the relationship between optical luminosity and r_{BLR} (Dibai 1977; Kaspi et al. 2000; Bentz et al. 2006), masses of black holes are estimated from the virial theorem, $M = fr_{BLR}FWHM^2/G$, where G is the gravitational constant and f is the “virial factor” depending on the geometry and kinematics of the BLR and the inclination angle, θ_0 . Unfortunately with current technology it is impossible to directly observe the structure of the BLR. Therefore the

* E-mail: mohammadghayuri@gmail.com

true value of f for each object is unknown and we are required to use average virial factor, $\langle f \rangle$, to estimate the mass of super-massive black hole. Comparison of virial masses with independent estimates of black hole masses using to $M - \sigma$ relationship (see Kormendy & Ho 2013) have given empirical estimates of the value of $\langle f \rangle$. However each study has found different value for $\langle f \rangle$. For example Onken et al. (2004) calculate $\langle f \rangle = 5.5 \pm 1.8$, Woo et al. (2010) calculate $\langle f \rangle = 5.2 \pm 1.2$, Graham et al. (2011) calculate $\langle f \rangle = 3.8_{-0.6}^{+0.7}$ and Grier et al. (2013) calculate $\langle f \rangle = 4.31 \pm 1.05$. This is because each group take a different sample. Different values for $\langle f \rangle$ prevent us to have a reliable value for black hole mass.

The situation for low-luminosity AGNs (LLAGNs) is somewhat different. The lack of broad optical emission lines in the faintest cases ($L = 10^{-9} < L < 10^{-6} L_{Edd}$) has led to two scenarios about the presence of BLR in LLAGNs. The first, which is somewhat supported by the theoretical models (e.g., Nicastro 2000; Elitzur & Shlosman 2006), simply says that the BLR is absent in such faint objects. However, there is clear evidence in favor of the presence of the BLR in some LLAGNs, at least those with $L > 10^{-5} L_{Edd}$. This supports a second scenario which says that the BLR exists in LLAGNs but we cannot detect them in the faintest cases because the intensity of their broad emission lines is below the detection threshold set mostly by starlight in the host galaxy. In the Palomar survey, it was found that broad H α emission is present in a remarkably high fraction of LINERs (LLAGNs)(see Ho 2008). Moreover, double-peaked broad emission lines have been found in some LINERs including NGC 7213 (Filippenko & Halpern 1984), NGC 1097 (Storchi-Bergmann et al. 1993), M81 (Bower et al. 1996), NGC 4450 (Ho et al. 2000) and NGC 4203 (Shields et al. 2000). Other studies have also shown the presence of variable broad emission lines for NGC 1097 (Storchi-Bergmann et al. 1993), M81 (Bower et al. 1996) and NGC 3065 (e.g., Eracleous & Halpern 2001). Recently, Balmaverde & Capetti (2014) found other LLAGNs with $L = 10^{-5} L_{Edd}$ showing BLRs.

Since the optical spectra of LLAGNs are severely contaminated by the host galaxy, some authors have suggested using the widths of the Paschen lines rather than Balmer lines to determine a FWHM (Landt et al. 2011, 2013; La Franca et al. 2015). Also, in order to estimate the BLR radius, r_{BLR} , we can use near-IR continuum luminosity at $1 \mu m$ (Landt et al. 2011, 2013) or X-ray luminosity (Greene et al. 2010) rather than the optical luminosity.

Whittle & Saslaw (1986) used the Boltzmann equation to describe the kinematics of BLR. More recently, Wang, Cheng & Li (2012) showed that the BLR can be considered as a collisionless ensemble of particles. By considering the Newtonian gravity of the black hole and a quadratic drag force, they used the collisionless Boltzmann equation (CBE) to study the dynamics of the clouds for the case where magnetic forces are unimportant. Following this approach, some authors included the effect of magnetic fields on the dynamics of the clouds in the BLR (e.g., Khajenabi et al. 2014). In this paper, we use the CBE to describe the distribution of the clouds in the BLR. The structure of this paper is as follows: in the section (2) we will establish our basic formalism and apply it in order to classify the clumpy structure of the BLR. In the section (3) we will concentrate on LLAGNs and give more details about the distribution of the clouds in such systems. Moreover, we will derive the virial factor f for them and in the final section, the conclusions are summarized.

2 KINEMATIC EQUATIONS OF CLOUDS IN THE BLR

This paper only considers axisymmetric, steady-state systems. In the subsection (2.1) we start by deriving the general form of the Jeans equations in cylindrical coordinates (R, ϕ, z) for a system of particles subject to velocity-dependent forces as well as position-dependent forces. Then, by assuming axisymmetry ($\partial/\partial\phi = 0$) and a steady state ($\partial/\partial t = 0$), we simplify the Jeans equations and use them to describe the distribution of the clouds in the BLR.

2.1 Jeans equations

If we define the distribution function F as $F = \Delta n/\Delta x \Delta y \Delta z \Delta^3 v$, the continuity equation in the phase space (see Binney & Tremaine 1987, eq 4.11) is given by $\partial F/\partial t + \sum_{\alpha=1}^6 \partial(F\omega_{\alpha})/\partial\omega_{\alpha} = 0$. This equation can be rewritten as $DF/Dt + F(\partial a_x/\partial v_x + \partial a_y/\partial v_y + \partial a_z/\partial v_z) = 0$ in Cartesian position-velocity space (x, y, z, v_x, v_y, v_z) where DF/Dt and \mathbf{a} are respectively the Lagrangian derivative in the phase space and the resultant acceleration vector. On the other hand by the chain rule, the partial derivatives with respect to the Cartesian components of the velocity are related to those respect to the cylindrical components by $\partial/\partial v_x = \cos\phi(\partial/\partial v_R) - \sin\phi(\partial/\partial v_{\phi})$, $\partial/\partial v_y = \sin\phi(\partial/\partial v_R) + \cos\phi(\partial/\partial v_{\phi})$ and $\partial/\partial v_z = \partial/\partial v_z$. Also the relationship between the Cartesian and cylindrical components of the acceleration vector is $a_x = a_R \cos\phi - a_{\phi} \sin\phi$, $a_y = a_R \sin\phi + a_{\phi} \cos\phi$ and $a_z = a_z$. Combining all of these equations, we obtain the extended form of the CBE in cylindrical position-velocity space ($R, \phi, z, v_R, v_{\phi}, v_z$) as

$$\frac{\partial F}{\partial t} + v_R \frac{\partial F}{\partial R} + \frac{v_{\phi}}{R} \frac{\partial F}{\partial \phi} + v_z \frac{\partial F}{\partial z} + \left(a_R + \frac{v_{\phi}^2}{R} \right) \frac{\partial F}{\partial v_R} +$$

$$\left(a_{\phi} - \frac{v_R v_{\phi}}{R} \right) \frac{\partial F}{\partial v_{\phi}} + a_z \frac{\partial F}{\partial v_z} + F \left(\frac{\partial a_R}{\partial v_R} + \frac{\partial a_{\phi}}{\partial v_{\phi}} + \frac{\partial a_z}{\partial v_z} \right) = 0. \quad (1)$$

As can be seen, in the absence of velocity-dependent forces, equation (1) agrees with the standard form (see Binney & Tremaine 1987, eq 4.15). As is shown in the Appendix A, the Jeans equations derived from equation (1) can be written as

$$\frac{\partial n}{\partial t} + \frac{1}{R} \frac{\partial}{\partial R} (nR \langle v_R \rangle) + \frac{1}{R} \frac{\partial}{\partial \phi} (n \langle v_{\phi} \rangle) + \frac{\partial}{\partial z} (n \langle v_z \rangle) = 0, \quad (2)$$

and

$$\begin{aligned} \frac{\partial}{\partial t} (n \langle v_R \rangle) + \frac{\partial}{\partial R} (n \langle v_R^2 \rangle) + \frac{1}{R} \frac{\partial}{\partial \phi} (n \langle v_R v_{\phi} \rangle) + \frac{\partial}{\partial z} (n \langle v_R v_z \rangle) \\ + n \frac{\langle v_R^2 \rangle - \langle v_{\phi}^2 \rangle}{R} - n \langle a_R \rangle = 0, \end{aligned} \quad (3)$$

and

$$\begin{aligned} \frac{\partial}{\partial t} (n \langle v_{\phi} \rangle) + \frac{\partial}{\partial R} (n \langle v_R v_{\phi} \rangle) + \frac{1}{R} \frac{\partial}{\partial \phi} (n \langle v_{\phi}^2 \rangle) + \frac{\partial}{\partial z} (n \langle v_{\phi} v_z \rangle) \\ + \frac{2n}{R} \langle v_{\phi} v_R \rangle - n \langle a_{\phi} \rangle = 0, \end{aligned} \quad (4)$$

and

$$\begin{aligned} \frac{\partial}{\partial t} (n \langle v_z \rangle) + \frac{\partial}{\partial R} (n \langle v_R v_z \rangle) + \frac{1}{R} \frac{\partial}{\partial \phi} (n \langle v_{\phi} v_z \rangle) + \frac{\partial}{\partial z} (n \langle v_z^2 \rangle) \\ + \frac{n \langle v_R v_z \rangle}{R} - n \langle a_z \rangle = 0, \end{aligned} \quad (5)$$

where n is the volume number density in the position-place. Equations (2) - (5) are an extended form of the Jeans equations describing a collisionless system of particles undergoing both velocity-dependent and position-dependent forces. Considering gravity as dominant force for a axisymmetric system of particles, equations (2) - (5) reduce to the standard form of the Jeans equations (see equations 4.28 and 4.29 of Binney & Tremaine 1987).

2.2 Dynamics and geometry of BLR

In this subsection, by considering a steady axisymmetric system, we include the Newtonian gravity of the black hole, the isotropic radiation pressure of the central source, and the drag force between the clouds and the ambient medium for the linear regime as the dominant forces. First we discuss about the role of radiation pressure and gravity and after that, through the analysis of the clouds near the midplane, we classify the distribution of the clouds in the BLR.

2.2.1 Radiation pressure versus gravity

Assuming that the clouds are optically thick, the radiative force can be expressed as

$$\mathbf{F}_{rad} = \frac{\sigma}{c} \mathcal{F} \mathbf{e}_r, \quad (6)$$

where σ and c are the cloud's cross-section and the speed of the light respectively, and the isotropic radiation flux, \mathcal{F} , is

$$\mathcal{F}(r) = \frac{L}{4\pi r^2}. \quad (7)$$

L is the bolometric luminosity of the central source and $r = \sqrt{R^2 + z^2}$ is the spherical radius. For the clouds near the midplane, $z \ll R$, the radiative force per unit of mass can be written as

$$\mathbf{a}_{Rad} = \Omega_{k,mid}^2 \frac{3l}{2\mu\sigma_T N_{cl}} (R\mathbf{e}_R + z\mathbf{e}_z), \quad (8)$$

where $\Omega_{k,mid} = \sqrt{GM/R^3}$ is the Keplerian angular velocity in the midplane, μ is the mean molecular weight, σ_T is the Thomson cross-section, l is the Eddington ratio, and N_{cl} is the column density of each cloud. Following previous studies, we consider the clouds, with conserved mass m_{cl} , in pressure equilibrium with the inter-cloud gas (e.g., Netzer & Marziani 2010; Krause et al. 2011; Khajenabi 2015). Furthermore, the pressure of the ambient medium, and hence the gas density in individual clouds, n_{gas} , are assumed to have a power-law dependence on the (spherical) distance from the centre as $n_{gas} \propto r^{-s}$. As a result, since $r \approx R$ for the clouds near the midplane, the column density defined by $N_{cl} = m_{cl}/R_{cl}^2$ finally becomes

$$N_{cl} = N_0 \left(\frac{R}{R_0} \right)^{-2s/3}, \quad (9)$$

where R_0 is one light day and N_0 is the column density at R_0 .

In addition to the gravitational and radiative forces, the drag force opposing relative movement of clouds and the ambient gas is another force that needs to be taken into consideration. Depending on the size of the clouds, there are two regimes for the drag force. These include the Epstein and the Stokes regimes (e.g., Armitage 2013). In the Epstein regime, which dominates for the small clouds, the magnitude of the force is proportional to the relative velocity. In the Stokes regime the drag affecting the movement of the large clouds increases as the square of the relative velocity. We assume the clouds have spherical shapes, so the drag coefficient in

the Stokes regime depends solely on the Reynolds number which is proportional to the relative velocity. Shadmehri (2015) demonstrated that the Reynolds number in the inter-cloud gas is lower than unity. This means that: (1) we can consider the inter-cloud gas as having a laminar flow and (2) the drag coefficient in the Stokes regime is proportional to the inverse of the Reynolds number (e.g., Armitage 2013). This means that the drag coefficient in the Stokes regime is proportional to the inverse of relative velocity. As a result, in both the Epstein and Stokes regimes, the magnitude of the drag force is proportional to the relative velocity and both small and large clouds are affected by a linear drag force as $\mathbf{F}_d = f_l(\mathbf{v} - \mathbf{w})$, where \mathbf{w} is the velocity of the ambient medium and f_l is the drag coefficient. The equations of motion of an individual cloud near the midplane are therefore given by

$$\begin{aligned} a_R &= -\Omega_{k,mid}^2 R \left[1 - \left(\frac{R}{R_c} \right)^{2s/3} \right] - f_l(v_R - w_R), \\ a_\phi &= -f_l(v_\phi - w_\phi), \\ a_z &= -\Omega_{k,mid}^2 z \left[1 - \left(\frac{R}{R_c} \right)^{2s/3} \right] - f_l(v_z - w_z), \end{aligned} \quad (10)$$

where R_c is the critical radius defined as

$$R_c = R_0 \left(\frac{2\mu\sigma_T N_0}{3l} \right)^{3/2s}. \quad (11)$$

From equations (8) and (9), we see that at $R = R_c$, the attractive gravitational and repulsive radiative force cancel each other and the magnitude of the resultant force is equal to zero. For $R > R_c$, the radiative force is stronger than gravity and accelerates the clouds away from the central black hole. For $R < R_c$ gravity overcomes the radiative force and pulls the clouds inwards. If we assume $s = 3/2$, $\mu = 0.61$, $l = 0.001$, $N_0 \approx 10^{23} \text{ cm}^{-2}$ and $\sigma_T = 6.7 \times 10^{-25} \text{ cm}^2$, the value of R_c almost becomes 27 light days which is in order of BLR radius (e.g., Krolik et al. 1991). Assuming a steady state and axisymmetry, we substitute equations (10) into equations (3) - (5) to obtain

$$\begin{aligned} \frac{\partial}{\partial R}(n\langle v_R^2 \rangle) + \frac{\partial}{\partial z}(n\langle v_R v_z \rangle) + n \frac{\langle v_R^2 \rangle - \langle v_\phi^2 \rangle}{R} \\ + n\Omega_{k,mid}^2 R \left[1 - \left(\frac{R}{R_c} \right)^{2s/3} \right] + n f_l(\langle v_R \rangle - w_R) = 0, \end{aligned} \quad (12)$$

and

$$\frac{\partial}{\partial R}(n\langle v_R v_\phi \rangle) + \frac{\partial}{\partial z}(n\langle v_\phi v_z \rangle) + \frac{2n}{R} \langle v_\phi v_R \rangle + n f_l(\langle v_\phi \rangle - w_\phi) = 0, \quad (13)$$

and

$$\begin{aligned} \frac{\partial}{\partial R}(n\langle v_R v_z \rangle) + \frac{\partial}{\partial z}(n\langle v_z^2 \rangle) + \frac{n\langle v_R v_z \rangle}{R} + n\Omega_{k,mid}^2 z \left[1 - \left(\frac{R}{R_c} \right)^{2s/3} \right] \\ + n f_l(\langle v_z \rangle - w_z) = 0. \end{aligned} \quad (14)$$

In this paper, we assume that the drag coefficients are sufficiently large that the clouds and the ambient medium are strongly coupled to each other. Thus we can write $\langle v_R \rangle = w_R$, $\langle v_\phi \rangle = w_\phi$ and $\langle v_z \rangle = w_z$. For simplicity we also assume $\langle v_z \rangle = 0$, $\langle v_R v_z \rangle = 0$

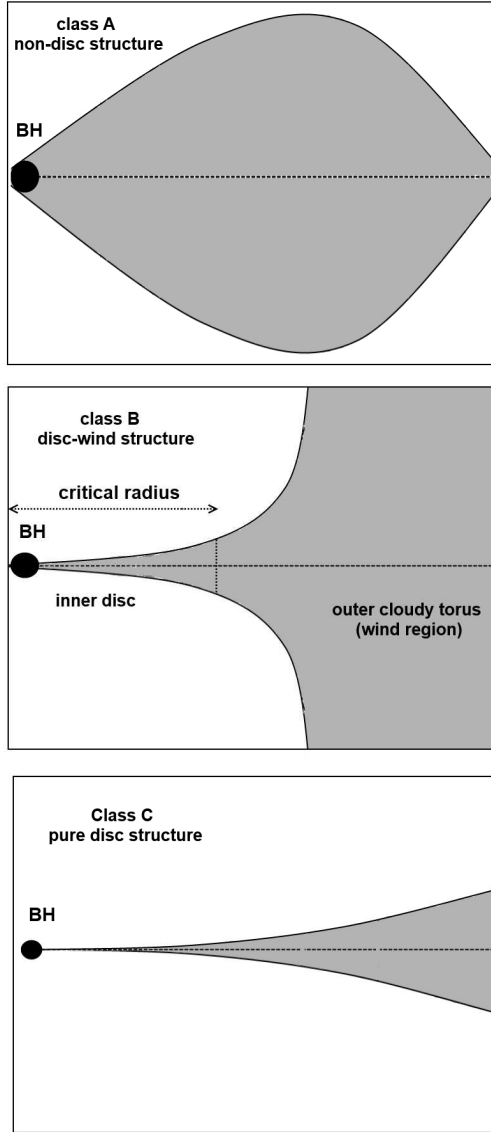


Figure 1. Classification of clumpy BLR structure. The black filled circle on the left shows the supermassive black hole. The grey and white areas show the clumpy and non-clumpy regions in the BLR respectively. The first panel shows class A in which the clouds occupy all positions in the BLR. The second panel shows class B. In this class we have a disc for $R < R_c$ and a cloudy torus (wind region) for $R > R_c$. The third panel shows class C in which the clumpy structure in the BLR is disc-like.

and $\langle v_\phi v_z \rangle = 0$. Therefore equations (2), (12), (13) and (14) are respectively reduced to

$$\frac{1}{R} \frac{\partial}{\partial R} (nR \langle v_R \rangle) = 0, \quad (15)$$

$$\frac{\partial}{\partial R} (n \langle v_R^2 \rangle) + n \frac{\langle v_R^2 \rangle - \langle v_\phi^2 \rangle}{R} + n \Omega_{k, mid}^2 R \left[1 - \left(\frac{R}{R_c} \right)^{2s/3} \right] = 0, \quad (16)$$

$$\frac{\partial}{\partial R} (n \langle v_R v_\phi \rangle) + \frac{2n}{R} \langle v_R v_\phi \rangle = 0, \quad (17)$$

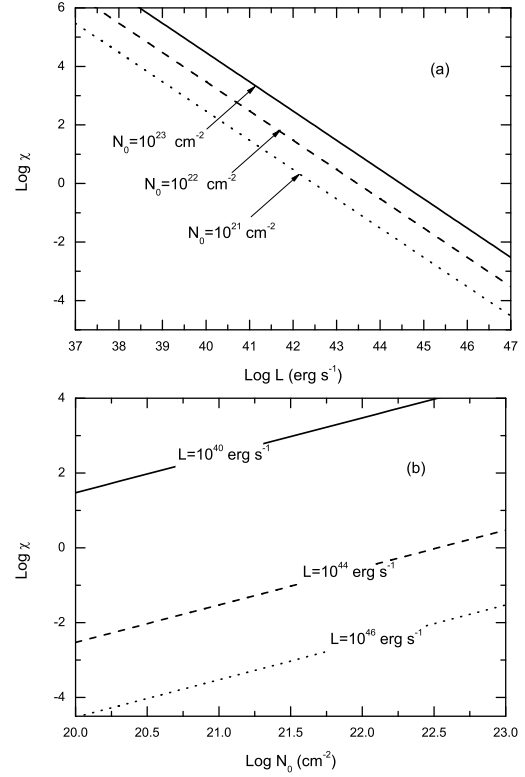


Figure 2. (a) $\log \chi$ versus $\log L$, for different values of the column density, N_0 . (b) $\log \chi$ versus $\log N_0$ for different values of the bolometric luminosity, L . In this Figure, $\log \chi < -2$ and $-2 < \log \chi < 0$ and $\log \chi > 0$ represents classes A, B, and C respectively.

and

$$\langle v_z^2 \rangle \frac{\partial n}{\partial z} + n \Omega_{k, mid}^2 z \left[1 - \left(\frac{R}{R_c} \right)^{2s/3} \right] = 0. \quad (18)$$

For simplicity $\langle v_z^2 \rangle$ is assumed to be constant in equation (18). Equation (18) shows while for $R < R_c$ we have $\partial n / \partial z < 0$ and most of the clouds are distributed near the midplane, for $R > R_c$ we have $\partial n / \partial z > 0$ and the clouds tend to be located in the higher altitudes. This result is quite in an agreement with what we discussed about R_c .

2.2.2 Classification of clumpy distribution

In this part we compare R_c with the innermost radius of the BLR R_{in} and the outermost radius R_{out} to show that there are three classes for clumpy distribution in the BLR:

Class A: $R_c < R_{in}$ and the clouds fill all positions in the intercloud gas (see the first panel in Figure 1).

Class B: $R_{in} < R_c < R_{out}$ and the clumpy structure is the combination of the inner disc extending from R_{in} to R_c and the outer cloudy torus (wind region) extending from R_c to R_{out} (see the second panel in Figure 1).

Class C: $R_c > R_{out}$ and the clumpy structure is disc-like (see the third panel in Figure 1).

Depending on the observational data which we know about each AGN we suggest three methods to find what category it belong to.

1) For some AGNs with black hole mass independently estimated from the $M - \sigma$ relationship (e.g., Onken et al. 2004;

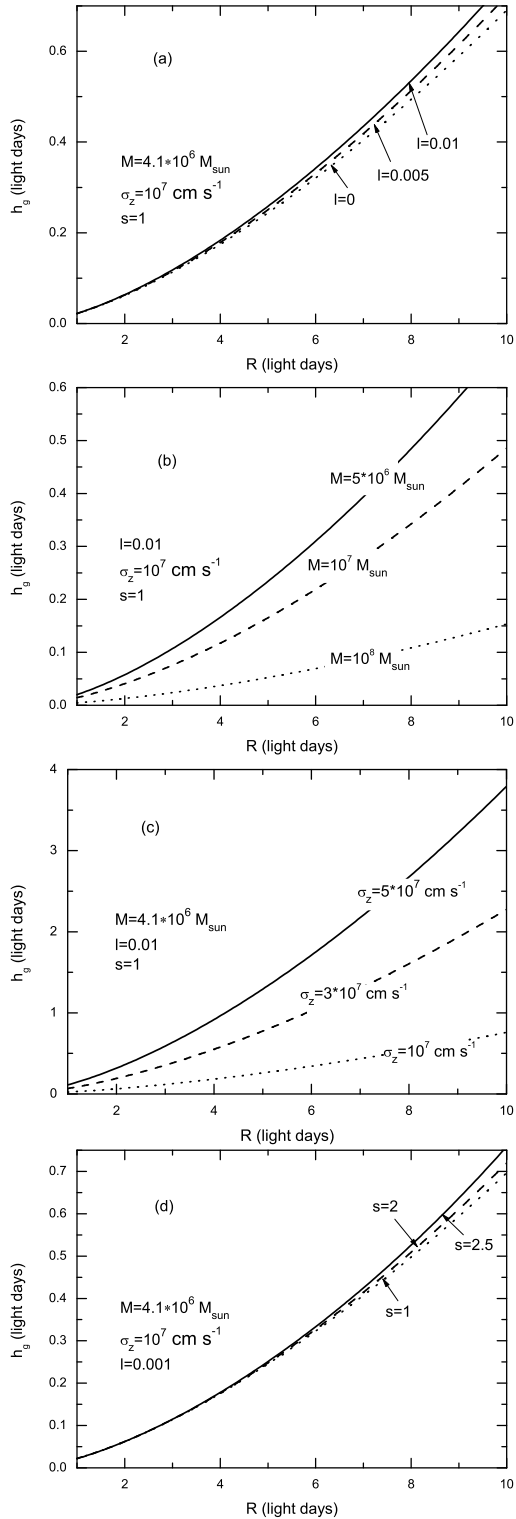


Figure 3. The scale height h_g versus the radial distance, R . The panels (a), (b), (c) and (d) respectively show the effect of the central luminosity, the black hole mass, z -component of the velocity dispersion and the density index on the geometric shape and thickness of the clumpy disc.

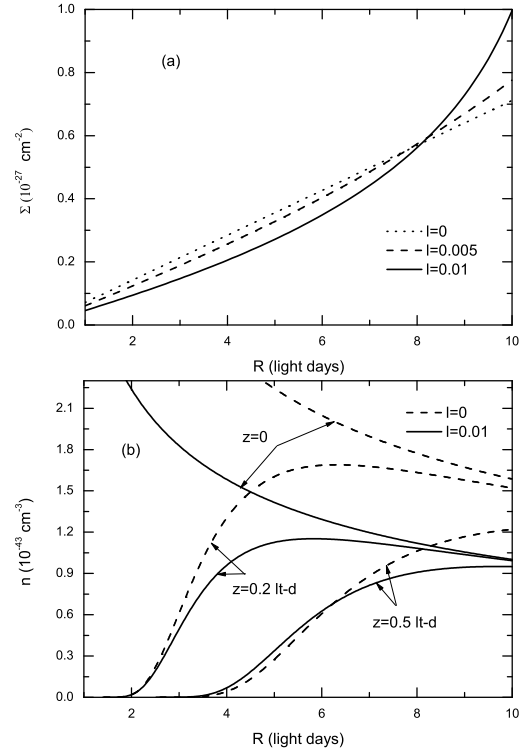


Figure 4. The distribution of BLR clouds for different values of the central luminosity. $M = 4.1 \times 10^6 M_\odot$, $\sigma_z = 10^7 \text{ cm/s}$, $s = 1$ and $n_{tot} = 10^6$. (a) The surface number density versus radial distance (b) The volume number density versus radial distance at $z = 0, 0.2$ and 0.5 light day (lt-d).

Woo et al. 2010; Graham et al. 2011; Grier et al. 2013), we can determine the Eddington luminosity defined by $L_{Edd} = 1.3 \times 10^{38} M/M_\odot \text{ erg/s}$. On the other hand, by measuring the bolometric luminosity, L , we have the Eddington ratio $l = L/L_{Edd}$. Also, we assume $1.2 \times 10^{21} \text{ cm}^{-2} < N_0 < 1.5 \times 10^{24} \text{ cm}^{-2}$ for the column density (e.g., Marconi et al. 2008) and $1 < s < 2.5$ (e.g., Rees et al. 1989). We can then calculate the value of R_c from equation (11) and compare it with R_{in} and R_{out} specified by reverberation mapping technique (e.g., Krolik et al. 1991) to determine what class each object belongs to.

2) For cases for which reverberation mapping is not available, the $R - L$ relationship (Kaspi et al. 2000; Bentz et al. 2006) can help us to estimate the BLR radius and compare it with R_c estimated by the method described above.

3) For AGNs with unknown black hole mass, if we assume $R_{in} = 10R_{Sch}$ and $R_{out} = 1000R_{Sch}$ we can define the parameter χ as $\chi = R_c/R_{out} = (0.005c^2 R_0/GM)(2\mu\sigma_T N_0/3l)^{3/2s}$. Clearly $\chi < 0.01$ implies $R_c < R_{in}$ and such systems belong to class A. Also, in the cases for which $0.01 < \chi < 1$ and $\chi > 1$, we see that they belong to the classes B and C respectively. Assuming that $s = 3/2$ we can combine the black hole mass with the Eddington ratio to get χ as

$$\chi = 4.89 \times 10^{21} \frac{\mu N_0}{L}. \quad (19)$$

The parameter χ derived from equation (19) can give the class of BLR structure for AGNs with unknown black hole mass. The top and bottom panels in Figure 2 show $\log \chi$ as a function of $\log L$ and $\log N_0$ respectively. In Figure 2 we can see that for quasars with luminosities ranging from 10^{44} erg/s to 10^{47} erg/s , we have $-2 < \log \chi < 0$ for less luminous systems and $\log \chi < -2$

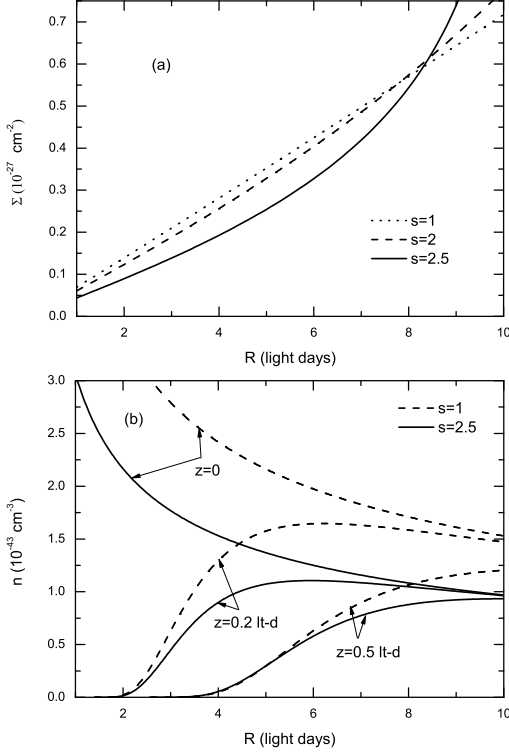


Figure 5. The distribution of BLR clouds for different density indices. $M = 4.1 \times 10^6 M_\odot$, $\sigma_z = 10^7 \text{ cm/s}$, $l = 10^{-4}$ and $n_{tot} = 10^6$. (a) The surface number density versus the radial distance, (b) The volume number density versus radial distance at $z = 0, 0.2$ and 0.5 light days (lt-d).

for the brightest cases. We therefore expect that the BLR structure of AGNs is similar to classes A and B for the higher and lower luminosity cases. For Seyfert galaxies with $10^{41} \text{ erg/s} < L < 10^{44} \text{ erg/s}$, the expected distribution of clouds is as in classes B and C for higher and lower luminosity objects. Finally for all the LLAGNs with $L < 10^{41} \text{ erg/s}$ we see $\log \chi$ is positive and BLR structure is as in class C (i.e., disc-like). Some studies, through a discussion on the shape of broad emission lines, have shown the existence of disc structure (class C) in LLAGNs (e.g., Eracleous & Halpern 2003; Storchi-Bergmann et al. 2016). Moreover they have found the existence of a non-disc region (outer torus in class B) in outer parts of BLR in Seyfert galaxies.

As the final step in this section, we solve equations (15) and (18) for the disc-like approximation to obtain the volume number density n . Because of the assumption of strong coupling between the BLR clouds and the hot intercloud medium we have $\langle v_R \rangle = w_R$. Furthermore, if we assume an advection-dominated accretion flow (ADAF) for the model describing the intercloud gas and because of the self-similar solution we can write $w_R = -\alpha c_1 v_{k,mid}$ (e.g., Narayan & Yi 1994), where α and c_1 are two constants in order of unity and $v_{k,mid}$ is the Keplerian velocity in the midplane. On the other hand, from equation (15) we can see that $nR\langle v_R \rangle$ does not depend on R , so

$$n(R, z) = -\frac{\Lambda(z)}{\alpha c_1 \sqrt{GM}} R^{-\frac{1}{2}}, \quad (20)$$

where $\Lambda(z)$ give the vertical dependence of n . By substituting equation (20) into equation (18) and after some algebraic manip-

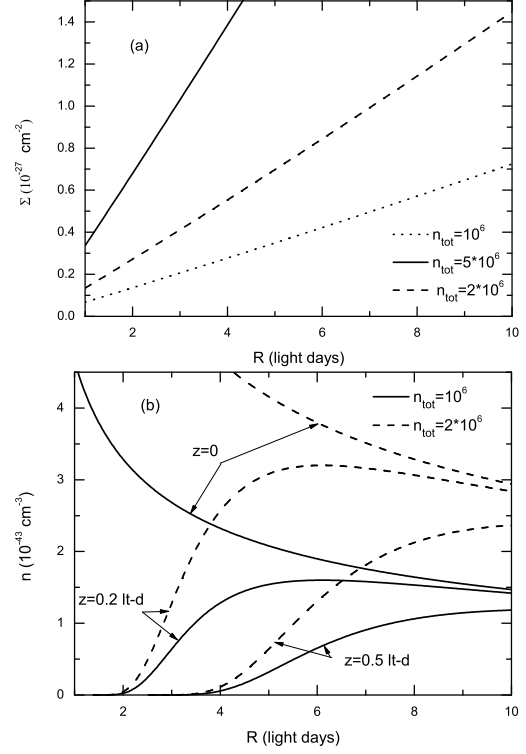


Figure 6. The distribution of BLR clouds for different values of the total number of the clouds. $M = 4.1 \times 10^6 M_\odot$, $\sigma_z = 10^7 \text{ cm/s}$, $l = 10^{-2}$ and $s = 1$. (a) Surface number density versus the radial distance (b) Volume number density versus the radial distance at $z = 0, 0.2$ and 0.5 light days (lt-d).

ulations, equation (18) can be written as

$$\langle v_z^2 \rangle \frac{\partial \Lambda(z)}{\partial z} + \Omega_{k,mid}^2 z \left[1 - \left(\frac{R}{R_c} \right)^{2s/3} \right] \Lambda(z) = 0. \quad (21)$$

If we substitute $\Lambda(z)$ derived by integrating equation (21) into equation (20), the volume number density is given by

$$n(R, z) = -\frac{k_0}{\alpha c_1 \sqrt{GM}} R^{-\frac{1}{2}} \exp\left(-\frac{z^2}{2h_g^2}\right), \quad (22)$$

where k_0 is the constant of integration and h_g is the scale height which is

$$h_g(R) = \frac{\sigma_z}{\Omega_{k,mid}} \sqrt{\frac{1}{1 - (R/R_c)^{2s/3}}}. \quad (23)$$

Integrating n over all positions occupied by the clouds, we calculate k_0 in terms of the total number of the cloud n_{tot} , and substitute it into equation (22) to derive n as

$$n(R, z) = \frac{\sqrt{GM}}{(2\pi)^{3/2} \sigma_z \gamma} n_{tot} R^{-1/2} \exp\left(-\frac{z^2}{2h_g^2}\right), \quad (24)$$

where $\sigma_z = \sqrt{\langle v_z^2 \rangle}$ is z -component of the velocity dispersion and γ is defined by $\gamma = \int_{R_{in}}^{R_{out}} \sqrt{1 - (R/R_c)^{2s/3}} R^2 dR$, and where R_{in} and R_{out} are assumed to be 1 and 10 light day respectively. To calculate the surface number density, Σ , we integrate equation (24) over z to get

$$\Sigma(R) = \frac{1}{2\pi} \frac{n_{tot}}{\gamma} R \sqrt{\frac{1}{1 - (R/R_c)^{2s/3}}}. \quad (25)$$

In all subsequent sections, we adopt $\mu = 0.61$.

3 VIRIAL FACTOR

3.1 Disc-like configurations

In the last section we saw that in class C we have a disc-like distribution for the BLR. There are now two questions: what is the geometric shape of the clumpy disc? and is its thickness small compared to its radial sizes? In this section, we will answer to these questions and explore the role of various physical parameters on the shape and thickness of the clumpy disc. According to equation (24) we consider the curved surface $z = h_g(R)$ as the boundary between the clumpy and non-clumpy regions. Through plotting the scale height profile as a function of the radial distance in Figure 3 we show the geometric shape of the clumpy disc.

In Figure 3, we see that there is a positive correlation between the radial distance and scale height. Panels a and b show the role of the central luminosity and black hole mass on the thickness of the clumpy disc respectively. From these we see that with an increase in the central luminosity, the disc thickness increases, and that an increase in the black hole mass leads to a decrease in thickness. This is because as l increases, radiative pressure dominates and pushes the clouds away from the midplane. However, an increase in the black hole mass leads to an increase in the gravitational attraction pulling the clouds toward the midplane. Panels c and d show that there is similar behaviour for h_g as a function of σ_z and s . With increases in both of them, h_g increases as well. Figure (3) also shows that, as suggested by some authors (e.g., Dumont & Collin-Souffrin 1990b; Goad et al. 2012), the clumpy disc is flared (bowl-shaped). The thickness of the clumpy disc is small compared to the radial size ($h_g \approx 0.1R$). This is important.

Obviously, as the central luminosity declines, the clouds exposed to this radiation reprocess less amount of energy. As a result the broad emission lines are weak in LLAGNs. However, in addition to this, the small thickness of the clumpy disc results in a small solid angle being covered by the clumpy disc and this leads to little capture of the central radiation. The fraction of radiation captured is given by $d\Omega/4\pi \approx \Theta^2/2 \approx h_g^2/2R^2$ which is of the order of 10^{-3} , where $d\Omega$ is the solid angle covered by the clumpy disc and $\Theta \approx h_g/R$. Therefore, all the clouds located in the BLR of LLAGN can only receive 0.001 of the central radiation which itself is in order of $10^{-4} - 10^{-5}$ the Eddington luminosity and this leads to the presence of very weak broad emission lines in the spectra of LLAGNs. In the very lowest luminosity cases ($L = 10^{-8} - 10^{-9} L_{Edd}$), the small thickness of the clumpy disc together with the faintness of the central source can cause that the broad emission lines to fall below observational detection thresholds and this can explain the lack of detection of any broad emission lines in such faint objects.

Figures 4, 5 and 6 respectively clarify the effect of l , s and n_{tot} on the surface number density Σ and volume number density n which are plotted versus the radius R . In these three figures, the first panels present the behaviour of Σ versus R and the second panels show the variations of n with radius at $z = 0, 0.2$ and 0.5 light day (lt-d). Values of the fixed parameters are specified in the captions. In these figures, the profiles of the surface number density show that most of the clouds are located in the outer parts of the BLR. However the profiles of the volume number density are somewhat different. Whilst in the midplane most of the clouds are close to the central black hole, at $z = 0.2$ lt-d, the value of n in the central

parts is almost zero and with increasing the radius, it increases to a maximum and then, for larger radial distances n gradually declines. At $z = 0.5$ lt-d the behaviour of the curve is similar to that at $z = 0.2$ lt-d but the peak of the curve moves towards radii. Note that, by considering the positive correlation between h_g and R , there is no contradiction between the behaviour of Σ and n as a function of R .

Panel 4a shows that as l increases, the ratio of the clouds in the outer regions of the BLR to those in the inner regions increases as well. On the other hand, by assuming strong coupling between the clouds and the ambient medium, we have $\langle v_\phi \rangle = w_\phi \propto v_{k,mid}$ and $\langle v_R \rangle = w_R \propto v_{k,mid}$. Consequently, we conclude that, with increasing of l , the number of slowly moving clouds in the outer parts increases and the number of quickly-moving clouds in the inner parts is reduced. In other words, as obtained by Netzer & Marziani (2010), we expect that with increasing l , the width of broad emission lines FWHM decreases. Panel 4b shows that an increase in l leads to the reduction in the number of the clouds near the midplane. This is because they are distributed to higher altitudes. As is shown in Figure 5 the effect of the density index is similar to that of the central luminosity. Finally, in Figure 6 we see that an increase in the total number of the clouds leads, as is expected, to an increase in the value of Σ and n .

3.2 Calculation of Virial factor for disc-like structure

We can derive the virial factor, f , for the disc-like clumpy structure as a function of the kinematic parameters of the BLR and the inclination angle (the angle between the observer's line of sight and the axis of symmetry of the thin-disc. In Appendix B, we will show that the averaged line of sight velocity square $\langle v_n^2 \rangle_{avr}$ can be written as

$$\langle v_n^2 \rangle_{avr} = \frac{1+\beta}{2} \langle v_R^2 \rangle \sin^2 \theta_0 + \langle v_z^2 \rangle \cos^2 \theta_0, \quad (26)$$

where θ_0 is the inclination angle and $\beta = \langle v_\phi^2 \rangle / \langle v_R^2 \rangle$ is taken to be constant. As in section (2), if we assume $\langle v_z \rangle = 0$, we have $\langle v_z^2 \rangle = \sigma_z^2$ which is taken to be constant. However, $\langle v_R^2 \rangle$ has to be derived by solving equation (16). Dividing equation (16) into n , we can write

$$\frac{\partial \langle v_R^2 \rangle}{\partial R} + \left[\frac{\partial \ln(n)}{\partial R} + \frac{1-\beta}{R} \right] \langle v_R^2 \rangle = -\Omega_{k,mid}^2 R \left[1 - \left(\frac{R}{R_c} \right)^{\frac{2s}{3}} \right], \quad (27)$$

where $\partial \ln(n)/\partial R$ is derived by the substitution of $n(R, z)$, from equation (24). Equation (27), as a first order differential equation, then becomes

$$\frac{\partial \langle v_R^2 \rangle}{\partial R} + \left[\frac{1-2\beta}{2R} + \frac{z^2}{h_g^3} \frac{dh_g}{dR} \right] \langle v_R^2 \rangle = -\Omega_{k,mid}^2 R \left[1 - \left(\frac{R}{R_c} \right)^{\frac{2s}{3}} \right]. \quad (28)$$

Finding the integrating factor, we can write the solution of equation (28) as

$$\langle v_R^2 \rangle = -GM R^{\frac{2\beta-1}{2}} \exp\left(\frac{z^2}{2h_g^2}\right) \int R^{-\frac{3+2\beta}{2}} \left[1 - \left(\frac{R}{R_c} \right)^{\frac{2s}{3}} \right] \times \exp\left(-\frac{z^2}{2h_g^2}\right) dR. \quad (29)$$

In this integral, the range of the variation of $\exp(-z^2/2h_g^2)$ as a function of R , is given by $[\partial \exp(-z^2/2h_g^2)/\partial R] \Delta R \approx \exp(-z^2/2h_g^2) (z^2/h_g^3) (h_g/R) \Delta R$ which is in the order of unity. This is because, in thin disc, we have $z \approx h_g$ and $\Delta R \approx R$. On the

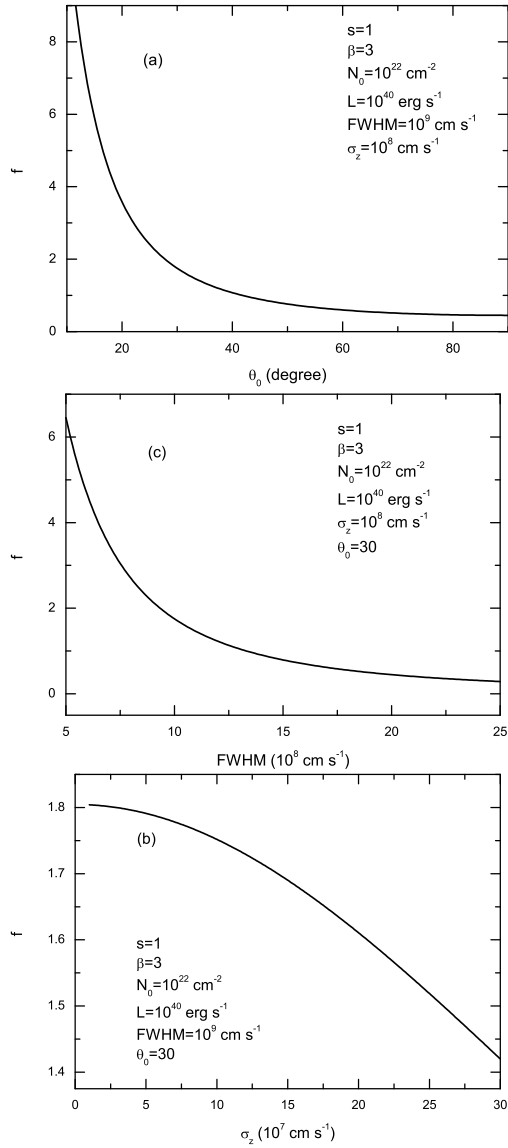


Figure 7. The panels (a), (b) and (c) show the virial factor as a function of inclination angle θ_0 , z-component of the velocity dispersion σ_z , and width of broad emission line FWHM respectively. Values of other fixed parameter are listed on each panel.

other hand, by assuming $R_{out} \approx 10R_{in}$, $\beta = 3$ and $s = 3/2$, we see that, as R increases from R_{in} to R_{out} , the value of the other terms inside the integral, $R^{-(3+2\beta)/2} [1 - (R/R_c)^{2s/3}]$, becomes smaller by a factor of 1000. We therefore assume that the value of $\exp(-z^2/2h_g^2)$ remains constant and by taking it out of the integral, $\langle v_R^2 \rangle$ is given by

$$\langle v_R^2 \rangle = \frac{GM}{R} \left[\frac{2}{1+2\beta} + \frac{6}{4s-6\beta-3} \left(\frac{R}{R_c} \right)^{\frac{2s}{3}} \right] + c_0, \quad (30)$$

where c_0 is the constant of integration calculated as follows. As we discussed in the subsection (2.2), for the thin-disc structure, we have $R < R_c$. As a result, in order to find the value of c_0 , we suppose that $\langle v_R^2 \rangle + \langle v_\phi^2 \rangle = (1 + \beta) \langle v_R^2 \rangle \approx 2FWHM^2$ at $R = 0.5R_c$. Finally, by substituting the constant of the integration into

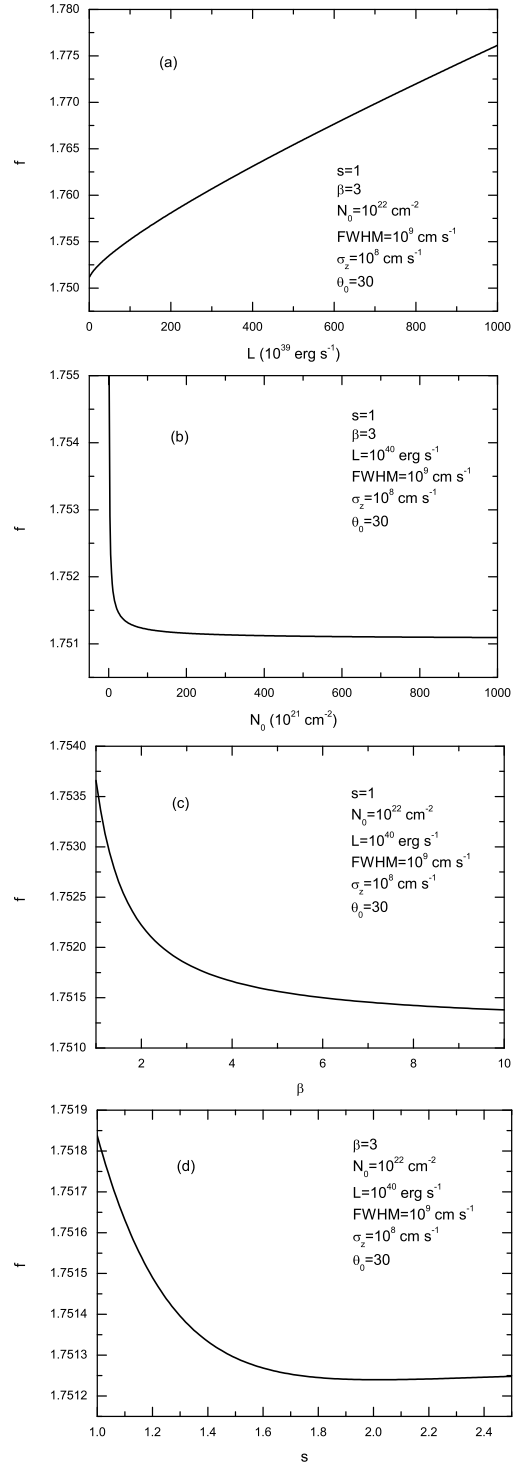


Figure 8. The panels (a), (b), (c) and (d) show the virial factor as a function of bolometric luminosity (L), column density (N_0), β and the density index (s) respectively. Values of other fixed parameter are listed on each panel.

equation (30), $\langle v_R^2 \rangle$ can be expressed as

$$\langle v_R^2 \rangle = \frac{GM}{R} \left\{ \left[\frac{2}{1+2\beta} + \frac{6}{4s-6\beta-3} \left(\frac{R}{R_c} \right)^{2s/3} \right] - \left[\frac{4}{1+2\beta} \right] \right.$$

$$+ \frac{12}{4s - 6\beta - 3} \left(\frac{1}{2} \right)^{2s/3} \left(\frac{R}{R_c} \right) \left. + \frac{2}{1 + \beta} \frac{R}{GM} \text{FWHM}^2 \right\}. \quad (31)$$

By substituting $\langle v_R^2 \rangle$ into equation (26), the virial factor defined by $f = GM/R\langle v_n^2 \rangle_{avr}$, is given by

$$f = \left\{ \left[\left(\frac{1 + \beta}{1 + 2\beta} + \frac{3 + 3\beta}{4s - 6\beta - 3} \left(\frac{R}{R_c} \right)^{2s/3} \right) - \left(\frac{2 + 2\beta}{1 + 2\beta} + \frac{6 + 6\beta}{4s - 6\beta - 3} \left(\frac{1}{2} \right)^{2s/3} \left(\frac{R}{R_c} \right) \right) + \frac{R}{GM} \text{FWHM}^2 \right] \sin^2 \theta_0 + \frac{R}{GM} \sigma_z^2 \cos^2 \theta_0 \right\}^{-1}. \quad (32)$$

Finally, assuming $R \approx R_{out} \approx 1000R_{Sch}$, the virial factor becomes

$$f = \left\{ \left[\left(\frac{1 + \beta}{1 + 2\beta} + \frac{3 + 3\beta}{4s - 6\beta - 3} \right) \chi^{-\frac{2s}{3}} - \left(\frac{2 + 2\beta}{1 + 2\beta} + \frac{6 + 6\beta}{4s - 6\beta - 3} \left(\frac{1}{2} \right)^{\frac{2s}{3}} \right) \chi^{-1} + 2000 \left(\frac{\text{FWHM}}{c} \right)^2 \right] \sin^2 \theta_0 + 2000 \left(\frac{\sigma_z}{c} \right)^2 \cos^2 \theta_0 \right\}^{-1}, \quad (33)$$

where $\chi = R_c/R_{out}$ is defined by equation (19).

Figures (7) and (8) show the variation of the virial factor as a function of the various parameters. In spite of all the approximations we have used, we see that the value of f is of the order of unity. This is in an agreement with previous works (e.g., Onken et al. 2004; Woo et al. 2010; Graham et al. 2011; Grier et al. 2013). Figure (7) shows that the virial factor changes significantly with the inclination angle θ_0 , the width of broad emission lines FWHM, and z -component of the velocity dispersion σ_z . From the first panel of Figure (7), it can be seen that as θ_0 increases from 0 to 40 (type1 AGNs), the value of f rapidly falls from nearly 9.0 to 1.0 and with increasing θ_0 from 40 to 90 (type2 AGNs), it gradually decreases from nearly 1.0 to 0.5. The negative correlation between f and θ_0 is similar to the finding derived by Pancoast et al. (2014) for five Seyfert galaxies including: Arp 151, Mrk 1310, NGC 5548, NGC 6814 and SBS 1116+583A. In the second panel of Figure (7) showing similar behaviour for the virial factor as a function of FWHM, we see $0.5 \lesssim f \lesssim 6.5$. The anticorrelation between f and FWHM has been confirmed by Brotherton et al. (2015). Finally the third panel shows that the value of f is nearly between 1.4 to 1.8. However, unlike two first panels, the slope of the curve in $f - \sigma_z$ diagram is shallow for lower values of σ_z and steep for higher values.

From Figure (8) we see that with increasing β , s and N_0 the value of the Virial factor, f , decreases and with increasing L it increases. But we have to note that the range of variation of f is so small (of the order of 0.01 for the variation of L and 0.001 for the variation of three other quantities). In other words, f is relatively insensitive to the variation of L , β , s and N_0 . The insensitive correlation between the Virial factor and bolometric luminosity is in agreement with the results found by Netzer & Marziani (2010). They found that while cloud orbits are strongly affected by radiation pressure, there is a relatively small change in $r_{BLR} \text{FWHM}^2$. This means that radiation pressure does not change the value of virial factor significantly.

4 CONCLUSIONS

In this work, considering the clouds as a collisionless ensemble of particles, we employed the cylindrical form of Jeans equations calculated in section 2 to describe a geometric model for their distributions in the BLR. The effective forces in this study are the Newtonian gravity of the black hole, the isotropic radiative force arisen from the central source and the drag force for linear regime. Taking them into account we showed that there are three classes for BLR configuration: (A) non disc (B) disc-wind (C) pure disc structure (see Figure 1). We also found that the distribution of BLR clouds in the brightest quasars belongs to class A, in the dimmer quasars and brighter Seyfert galaxies it belongs to class B, and in the fainter Seyfert galaxies and all LLAGNs (LINERs) it belongs to class C.

Then we derived the Virial factor, f , for disc-like structures and found a negative correlation for f as a function of the inclination angle, the width of broad emission line and z -component of the velocity dispersion. We also found $1.0 \lesssim f \lesssim 9.0$ for type1 AGNs and $0.5 \lesssim f \lesssim 1.0$ for type2 AGNs. Moreover we saw that f approximately varies from 0.5 to 6.5 for different values of FWHM and from 1.4 to 1.8 for different values of σ_z . We also indicated that f doesn't change significantly with the variations of bolometric luminosity, column density of each cloud, density index and $\beta = \langle v_\phi^2 \rangle / \langle v_R^2 \rangle$ and the maximum change in the value of f is of order of 0.01.

In introduction, we mentioned that since each group take a different sample of AGNs, they find different values for average virial factor, $\langle f \rangle$. However different values leads to significant uncertainties in the estimation of black hole mass. On the other hand, in this paper, we saw that f significantly changes with the inclination angle θ_0 and FWHM (Figure 7). Therefore in order to have more accurate estimation for black hole mass, we suggest observational campaigns to divide a sample of objects into a few subsamples based on the value of θ_0 and FWHM of objects and then determine the value of $\langle f \rangle$ for each subsample separately. Therefore we will have several values for $\langle f \rangle$. Finally regarding the value of θ_0 and FWHM of each object with unknown black hole mass, we use the appropriate value of $\langle f \rangle$ in the virial theorem to have more accurate estimation of black hole mass.

ACKNOWLEDGEMENTS

I am very grateful to the referee, Jian-Min Wang, for his very useful comments which improved the manuscript. I also thank Scott Tremaine for his useful suggestions that clarified some points about the extended form of the collisionless Boltzmann equation.

REFERENCES

- Armitage P. J., 2013, *Astrophysics of Planet Formation*, Cambridge University Press
- Balmaverde B., Capetti A., 2014, *A&A*, 563, A119
- Bentz M. C., Peterson B. M., Pogge R. W., Vestergaard M., Onken C. A., 2006, *ApJ*, 644, 133
- Binney J., Tremaine S., 1987, *Galactic dynamics*, Princeton, NJ, Princeton University Press (BT)
- Blanford R. D., & McKee, C. F. 1982, *ApJ*, 255, 419
- Bon E., Popovic L. C., Gavrilovic N., La Mura G., Mediavilla E., 2009, *MNRAS*, 400, 924
- Brotherton M. S., Singh V., Runnoe J., 2015, *MNRAS*, 454, 3864

- Bower G. A., Wilson A. S., Heckman T. M., & Richstone D. O. 1996, *AJ*, 111, 1901
- Chen K. & Halpern, J.P. 1989, *ApJ*, 344, 115.
- Chen K., Halpern, J.P. & Filippenko, A.V. 1989, *ApJ*, 339, 742.
- Dibai E. A. 1977, *Soviet Astron. Lett.*, 3, 1
- Dumont A.M. & Collin-Souffrin, S. 1990a, *A&AS* 83, 71.
- Dumont, A. M., & Collin-Souffrin, S. 1990b, *A&A*, 229, 313
- Elitzur M. & Shlosman, I. 2006, *ApJ*, 648, L101
- Eracleous M. & Halpern, J.P. 1994, *ApJS*, 90, 1.
- Eracleous M., Halpern J. P., 2001, *ApJ*, 554, 240
- Eracleous M. & Halpern, J.P. 2003, *ApJ*, 599, 886.
- Filippenko A. V., Halpern J. P., 1984, *ApJ*, 285, 458
- Gaskell C. M., Sparke L. S., 1986, *ApJ*, 305, 175
- Gaskell C.M., 2009, *NewAR*, 53, 140
- Goad M. R., Korista, K. T., & Ruff, A. J. 2012, *MNRAS*, 426, 3086
- Graham A. W., Onken C. A., Athanassoula E., & Combes F. 2011, *MNRAS*, 412, 2211
- Greene J. E., Hood C. E., Barth A. J., Bennert V. N., Bentz M. C., Filippenko A. V., Gates E., Malkan M. A., Treu T., Walsh J. L., Woo J.-H., 2010, *ApJ*, 723, 409
- Grier C.J., Martini P., Watson, L.C., Peterson B.M., Bentz M.C., Dasyra K.M., Dietrich M., Ferrarese L., Pogge R.W. & Zu, Y. 2013, *ApJ*, 773, 90
- Ho L. C., Rix H.-W., Shields J. C., Rudnick G., McIntosh D. H., Filippenko A. V., & Sargent W. L. W. , & Eracleous, M. 2000, *ApJ*, 541, 120
- Ho L. C., 2008, *ARA&A*, 46, 475
- Kaspi S., Smith P.S., Netzer H., Maoz D., Jannuzi B.T., Giveon U., 2000, *ApJ*, 533, 631
- Khajenabi F., Rahmani M., Abbassi S., 2014, *MNRAS*, 439, 2468
- Khajenabi F., 2015, *MNRAS*, 446, 1848
- Kollatschny W. & Bischoff, K. 2002, *A&A*, 386, L19.
- Kollatschny W. 2003, *A&A*, 407, 461
- Kormendy J., Ho L. C., 2013, *ARA&A*, 51, 511
- Krause M., Burkert A., Scharfmann M., 2011, *MNRAS*, 411, 550
- Krolik J. H., Horne Keith., Kallman T. R., Malkan M. A., Edelson R. A., Kriss, G. A. 1991, *ApJ*, 371, 541
- La Franca F., Onori F., Ricci F., Sani E., Brusa M., Maiolino R., Bianchi S., Bongiorno A., Fiore F., Marconi A., Vignali C. 2015, *MNRAS*, 449, 1526
- Landt H., Elvis M., Ward M. J., Bentz M. C., Korista K. T., Karovska M., 2011, *MNRAS*, 414, 218
- Landt H., Ward M. J., Peterson B. M., Bentz M. C., Elvis M., Korista K. T., Karovska M., 2013, *MNRAS*, 432, 113
- Marconi A., Axon D. J., Maiolino R., Nagao T., Pastorini G., Pietrini P., Robinson A., Torricelli G., 2008, *ApJ*, 678, 693
- Narayan R., Yi I., 1994, *ApJ*, 428, L13
- Netzer H., Marziani P., 2010, *ApJ*, 724, 318
- Nicastro F. 2000, *ApJ*, 530, L65
- Onken C. A., Ferrarese, L., Merritt, D., Peterson, B. M., Pogge, R. W., Vestergaard, M., & Wandel, A. 2004, *ApJ*, 615, 645
- Pancoast Anna., Brewer Brendon J., Treu Tommaso., Park Dae-seong., Barth Aaron J., Bentz Misty C., Woo Jong-Hak., 2014, *MNRAS*, 445, 3073
- Peterson B. M. 1993, *PASP*, 105, 247
- Peterson B. M., Ferrarese, L., Gilbert, K. M., et al. 2004, *ApJ*, 613, 682
- Popovic L. C., Mediavilla E., Bon E., Ilic D., 2004, *A&A*, 423, 909
- Rees M. J., Netzer H., Ferland G. J., 1989, *ApJ*, 347, 640
- Shadmehri., 2015, *MNRAS*, 451.3671
- Shields, J. C. et al. 2000, *ApJ*, 534, L27
- Smith J. E., Robinson A., Young S., Axon D. J., Corbett E. A., 2005, *MNRAS*, 359, 846
- Storchi-Bergmann T., Baldwin J. A., & Wilson A. S., 1993, *ApJ*, 410, L11
- Storchi-Bergmann T., Schimoia J.S., Peterson B.M., Elvis M., Denney K.D., Eracleous M., Nemmen R. S., 2016, submitted to *ApJ*
- Strateva I.V., Strauss, M.A., Hao, L. et al. 2003, *AJ*, 126, 1720
- Wang J.-M., Cheng C., Li Y.-R., 2012, *ApJ*, 748, 147
- Whittle M., Saslaw W. C., 1986, *ApJ*, 310, 104
- Woo J.-H., Treu, T., Barth, A. J., et al. 2010, *ApJ*, 716, 269

APPENDIX A: DERIVATION OF JEANS EQUATION

In this appendix, we derive the Jeans equations from the collisionless Boltzmann equation (CBE) for the particles which their movements are affected by both position-dependent and velocity dependent forces. First we demonstrate the mathematical formula which is used in this way several times. From the Product Rule for Derivatives, we have

$$\int \psi \frac{\partial F}{\partial v_i} d^3 v = \int \frac{\partial(\psi F)}{\partial v_i} d^3 v - \int F \frac{\partial \psi}{\partial v_i} d^3 v, \quad (\text{A1})$$

where, ψ , and F are an arbitrary function and the distribution function respectively. Moreover v_i represents the velocity components in the cylindrical coordinates (v_R, v_ϕ, v_z) . Since we don't have any particle with infinite velocity, so the value of F for sufficiently large velocities is equal to zero (e.g., Binney & Tremaine 1987) and, due to the divergence theorem, the first term on the right side of equation (A1) vanishes and we have

$$\int \psi \frac{\partial F}{\partial v_i} d^3 v = - \int F \frac{\partial \psi}{\partial v_i} d^3 v. \quad (\text{A2})$$

On the other hand, we define the averaged parameter in the velocity space as $\langle X \rangle = n^{-1} \int X F d^3 v$ where X is an arbitrary parameter and n is the volume number density in position-place which is calculated by $n = \int F d^3 v$. Integrating CBE in the velocity space, we have

$$\begin{aligned} & \int \frac{\partial F}{\partial t} d^3 v + \int v_R \frac{\partial F}{\partial R} d^3 v + \int \frac{v_\phi}{R} \frac{\partial F}{\partial \phi} d^3 v + \int v_z \frac{\partial F}{\partial z} d^3 v \\ & + \int \left(a_R + \frac{v_\phi^2}{R} \right) \frac{\partial F}{\partial v_R} d^3 v + \int \left(a_\phi - \frac{v_R v_\phi}{R} \right) \frac{\partial F}{\partial v_\phi} d^3 v \\ & + \int a_z \frac{\partial F}{\partial v_z} d^3 v + \int F \frac{\partial a_R}{\partial v_R} d^3 v + \int F \frac{\partial a_\phi}{\partial v_\phi} d^3 v + \int F \frac{\partial a_z}{\partial v_z} d^3 v = 0, \end{aligned} \quad (\text{A3})$$

since the velocity components (v_R, v_ϕ, v_z) don't depend on R , ϕ and z and also the range of velocities over which we integrate depends on neither time nor space, so the partial derivatives respect to both time $(\partial/\partial t)$ and space $(\partial/\partial R, \partial/\partial \phi, \partial/\partial z)$ in the first four terms on the left side of equation (A3) are taken outside. Also by using equation (A2) for the fifth, sixth and seventh terms of equation (A3), the first relation of the Jeans equations is gained as

$$\frac{\partial n}{\partial t} + \frac{1}{R} \frac{\partial}{\partial R} (Rn \langle v_R \rangle) + \frac{1}{R} \frac{\partial}{\partial \phi} (n \langle v_\phi \rangle) + \frac{\partial}{\partial z} (n \langle v_z \rangle) = 0, \quad (\text{A4})$$

the derivation of other relations of the Jeans equations is similar to that of the first one. By multiplying CBE by v_R, v_ϕ and v_z respectively and integrating them in the velocity-space, other equations can be given by

$$\begin{aligned} & \frac{\partial}{\partial t} (n \langle v_R \rangle) + \frac{\partial}{\partial R} (n \langle v_R^2 \rangle) + \frac{1}{R} \frac{\partial}{\partial \phi} (n \langle v_R v_\phi \rangle) + \frac{\partial}{\partial z} (n \langle v_R v_z \rangle) \\ & + n \frac{\langle v_R^2 \rangle - \langle v_\phi^2 \rangle}{R} - n \langle a_R \rangle = 0, \end{aligned} \quad (\text{A5})$$

and

$$\begin{aligned} & \frac{\partial}{\partial t} (n \langle v_\phi \rangle) + \frac{\partial}{\partial R} (n \langle v_R v_\phi \rangle) + \frac{1}{R} \frac{\partial}{\partial \phi} (n \langle v_\phi^2 \rangle) + \frac{\partial}{\partial z} (n \langle v_\phi v_z \rangle) \\ & + \frac{2n}{R} \langle v_\phi v_R \rangle - n \langle a_\phi \rangle = 0, \end{aligned} \quad (\text{A6})$$

and

$$\begin{aligned} & \frac{\partial}{\partial t} (n \langle v_z \rangle) + \frac{\partial}{\partial R} (n \langle v_R v_z \rangle) + \frac{1}{R} \frac{\partial}{\partial \phi} (n \langle v_\phi v_z \rangle) + \frac{\partial}{\partial z} (n \langle v_z^2 \rangle) \\ & + \frac{n \langle v_R v_z \rangle}{R} - n \langle a_z \rangle = 0. \end{aligned} \quad (\text{A7})$$

APPENDIX B: CALCULATION OF AVERAGED LINE OF SIGHT VELOCITY SQUARE

In this part, we calculate the averaged line of sight velocity square. We assume that the central black hole is placed at the origin of our coordinates system and $x - y$ plane is the midplane of the BLR. In this configuration, the velocity of the cloud placed at (R, ϕ, z) can be expressed as

$$\mathbf{v} = v_R \hat{R} + v_\phi \hat{\phi} + v_z \hat{z}, \quad (\text{B1})$$

where \hat{R} , $\hat{\phi}$ and \hat{z} are

$$\hat{R} = \cos \phi \hat{x} + \sin \phi \hat{y},$$

$$\hat{\phi} = -\sin \phi \hat{x} + \cos \phi \hat{y},$$

$$\hat{z} = \hat{z}. \quad (\text{B2})$$

On the other hand, the unit vector pointing towards the observer can be written as

$$\hat{n} = \sin \theta_0 \cos \phi_0 \hat{x} + \sin \theta_0 \sin \phi_0 \hat{y} + \cos \theta_0 \hat{z}, \quad (\text{B3})$$

where θ_0 is the inclination angle, and ϕ_0 determines the direction of \hat{n} . Therefore the line of sight velocity square defined by $v_n^2 = (\mathbf{v} \cdot \hat{n})^2$ becomes

$$\begin{aligned} v_n^2 &= v_R^2 \sin^2 \theta_0 \cos^2(\phi_0 - \phi) + v_\phi^2 \sin^2 \theta_0 \sin^2(\phi_0 - \phi) + v_z^2 \cos^2 \theta_0 \\ &+ 2v_R v_\phi \sin^2 \theta_0 \sin(\phi_0 - \phi) \cos(\phi_0 - \phi) + 2v_R v_z \sin \theta_0 \cos \theta_0 \cos(\phi_0 - \phi) \\ &+ 2v_\phi v_z \sin \theta_0 \cos \theta_0 \sin(\phi_0 - \phi). \end{aligned} \quad (\text{B4})$$

Like subsection (2.2) we assume $\langle v_R v_z \rangle = \langle v_\phi v_z \rangle = 0$. Thus $\langle v_n^2 \rangle$ is given by

$$\begin{aligned} \langle v_n^2 \rangle &= \langle v_R^2 \rangle \sin^2 \theta_0 \cos^2(\phi_0 - \phi) + \langle v_\phi^2 \rangle \sin^2 \theta_0 \sin^2(\phi_0 - \phi) \\ &+ \langle v_z^2 \rangle \cos^2 \theta_0 + 2 \langle v_R v_\phi \rangle \sin^2 \theta_0 \sin(\phi_0 - \phi) \cos(\phi_0 - \phi). \end{aligned} \quad (\text{B5})$$

Here we define the average of $\langle v_n^2 \rangle$ over the ϕ coordinate as $\langle v_n^2 \rangle_{avr} = (1/2\pi) \int_0^{2\pi} \langle v_n^2 \rangle d\phi$. By taking the average of equation (B5) and by using $\beta = \langle v_\phi^2 \rangle / \langle v_R^2 \rangle$, we can finally write $\langle v_n^2 \rangle_{avr}$ as

$$\langle v_n^2 \rangle_{avr} = \frac{1 + \beta}{2} \langle v_R^2 \rangle \sin^2 \theta_0 + \langle v_z^2 \rangle \cos^2 \theta_0. \quad (\text{B6})$$